Biochemical and Biophysical Research Communications 430 (2013) 265–271

Contents lists available at SciVerse ScienceDirect

Biochemical and Biophysical Research Communications

journal homepage: www.elsevier.com/locate/ybbrc

Crystal structure of the single cystathionine β-synthase domain-containing protein CBSX1 from *Arabidopsis thaliana* ☆

Byung-Cheon Jeong [a], Si Hoon Park [a], Kyoung Shin Yoo [b], Jeong Sheop Shin [a], Hyun Kyu Song [a,*]

[a] School of Life Sciences and Biotechnology, Korea University, Seoul 136-701, Republic of Korea
[b] College of Health Science, Korea University, Seoul 136-703, Republic of Korea

ARTICLE INFO

Article history:
Received 27 October 2012
Available online 14 November 2012

Keywords:
Arabidopsis thaliana
CBSX1
CBSX2
Cystathionine β-synthase domain
Plant
Thioredoxin

ABSTRACT

The single cystathionine β-synthase (CBS) pair proteins from *Arabidopsis thaliana* have been identified as being a redox regulator of the thioredoxin (Trx) system. CBSX1 and CBSX2, which are two of the six *Arabidopsis* cystathione β-synthase domain-containing proteins that contain only a single CBS pair, have close sequence similarity. Recently, the crystal structure of CBSX2 was determined and a significant portion of the internal region was disordered. In this study, crystal structures of full-length CBSX1 and the internal loop deleted (Δloop) form are reported at resolutions of 2.4 and 2.2 Å, respectively. The structures of CBSX1 show that they form anti-parallel dimers along their central twofold axis and have a unique ~155° bend along the side. This is different from the angle of CBSX2, which is suggestive of the flexible nature of the relative angle between the monomers. The biochemical data that were obtained using the deletion as well as point mutants of CBSX1 confirmed the importance of AMP-ligand binding in terms of enhancing Trx activity.

1. Introduction

Cystathionine β-synthase (CBS) domains are evolutionarily conserved small intracellular modules that are mostly found in two or four copies within a protein and have been identified in many proteins in all kingdoms of life [1]. The CBS domain or a CBS pair was first discovered in the archaebacteria *Methanococcus jannaschii* genome as a highly conserved domain of ~60 amino acids in various proteins [2]. A homology search analysis of protein databases revealed that this domain is also present in eubacterial and eukaryotic proteins with known specific functions. Functional analyses of point mutations in the CBS domains of enzymes and other proteins showed the physiological importance of the CBS pair, which, when mutated can seriously cripple specific protein functions thus causing several human hereditary diseases such as homocystinuria (cystathionine β-synthase deficiency) [3], Wolff-Parkinson-White syndrome (γ2 subunit of AMP-activated protein kinase) [4], retinitis pigmentosa (IMP dehydrogenase 1) [5], congenital myotonia, idiopathic generalized epilepsy, hypercalciuric nephrolithiasis, and classic Bartter syndrome (CLC, chloride channel family members) [1,2,6,7].

The structures of CBS domains in diverse proteins and isolated CBS domain-containing proteins (CDCPs) have been determined by X-ray crystallography: IMP dehydrogenase from *Streptococcus pyogenes* [8], AMP-activated kinases from yeasts and mammals [9–11], CBS from *Drosophila* [12], an Mg^{2+} transporter MgtE from *Thermus thermophilus* [13], Cl^- transporters from human and *Cyanidioschyzon merolae* [14], CBS domain-containing pyrophosphatase (CBS-PPase) from *Clostridium perfringens* [15], a zinc ribbon-like protein TA0289 from *Thermoplasma acidophilum* [16], MJ1225 and MJ0100 from *Methanocaldococcus jannaschii* [17,18], TM0935 from *Thermotoga maritima* [19], PAE2072 from *Pyrobaculum aerophilum* [20], ST2348 from *Sulfolobus tokodaii* [21], hypoxic response protein 1 from *Mycobacterium tuberculosis* [22], and CBSX2 from *Arabidopsis thaliana* [23]. Although the overall structures of the CBS domains are similar, unique structural features also exist. Interestingly, the regulatory role of the CBS module in multi-domain proteins is relatively well understood while the function of isolated CDCPs remains obscure due to a lack of information on their binding partners. In contrast to other eukaryotic systems, isolated CDCPs are more frequently found in plants [24].

Abbreviations: CBS, cystathionine β-synthase; CDCP, CBS domain-containing protein; MR, molecular replacement; RMS, root mean square; TEV, tobacco etch virus; Trx, thioredoxin.

☆ The atomic coordinates and structure factors (ID code: 4GQV and 4GQW) have been deposited in the Protein Data Bank (http://www.rcsb.org).

* Corresponding author. Address: School of Life Sciences and Biotechnology, Korea University, Anam-Dong, Seongbuk-Gu, Seoul 136-701, Republic of Korea. Fax: +82 2 3290 3628.
E-mail address: hksong@korea.ac.kr (H.K. Song).

0006-291X/$ - see front matter © 2012 Elsevier Inc. All rights reserved.
http://dx.doi.org/10.1016/j.bbrc.2012.10.139

Recent structural and functional studies on CDCPs from plants showed that they are easily detected by sequence analysis and are quite abundant (49 CBS domains were found in *A. thaliana*; http://pfam.sanger.ac.uk/family/PF00571). CBSX1 and CBSX2, which are two of the six *Arabidopsis* CDCPs that contain only a single CBS pair, interact with all types of Trxs. In addition, CBSX-mediated enhancement of Trx activity is further augmented by AMP [23]. The structure of homodimeric CBSX2 (PDB entry 3SL7) shows unique structural features, including an anti-parallel dimer along the central twofold axis, a flexible insertion loop followed by an additional α5 helix, and an approximately 125° bend in the overall shape along the side of the molecule [23]. CBSX1 crystals were obtained and several data sets were collected for MAD and MIR phasing [25]. However, the phase problem was not overcome with the data sets. In this study, crystal structures of full-length CBSX1 and the CBSX1 Δloop form that lacks the flexible internal region are reported at resolutions of 2.4 and 2.2 Å, respectively. Two structures showed that they exhibit the same folding, regardless of the flexible insertion loop and exist as an anti-parallel dimer along the central twofold axis but have different bending angles along the side. Therefore, these are unique features of single CDCPs from plants. The positively charged residues that form a putative AMP binding site were also identified and verified by a biochemical assay using mutants.

2. Materials and methods

2.1. Constructs and mutants

Genes encoding full-length CBSX1 (residue 71–236) without the signal sequence (Fig. 1A) were cloned into GST-tagged and/or His-

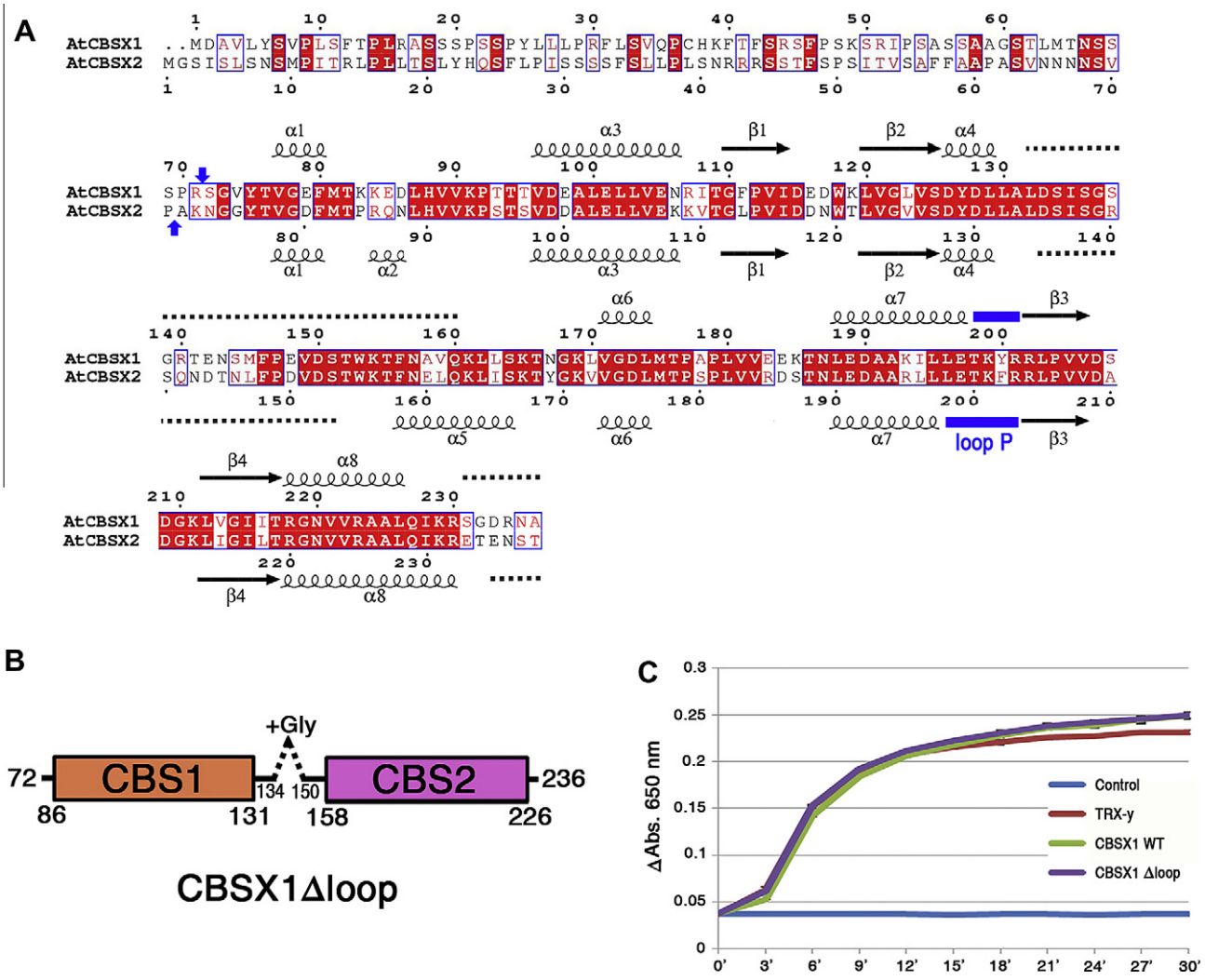

Fig. 1. (A) Sequence alignment between *A. thaliana* CBSX1 and CBSX2. The N-terminal signal sequence for targeting to chloroplasts is included in the alignment, and the predicted cleavage sites (as predicted by ChloroP server, http://www.cbs.dtu.dk/services/ChloroP/) are indicated by blue arrows. The secondary structural elements at the top and bottom of each alignment correspond to those of CBSX1 and CBSX2, respectively. Invisible segments in the structure are marked as black dots. The loop P is also indicated by a thick blue line and is labeled. Strictly conserved and conservatively substituted residues are boxed in red and white, respectively. Every 10th residue for CBSX1 and CBSX2 is indicated at the top and bottom of each alignment, respectively. (B) A schematic drawing of the CBSX1 Δloop (internal deletion mutant of CBSX1). The CBSX1 CBS1 and CBS2 domains are colored orange and violet, respectively. One glycine residue (represented as+Gly) is inserted to connect residue 134–residue 150 and is shown as a broken line. (C) The kinetic profile of the assay using insulin to follow the effects on Trx-y reducing activity by CBSX1 wild-type (WT) and the CBSX1 Δloop, where the difference in absorbance at 650 nm was measured every 3 min for 30 min. The profiles of the control, Trx-y only, Trx-y with CBSX1 WT, and Trx-y with the CBSX1 Δloop are shown as blue, red, green, and purple lines, respectively. The error bars were calculated based on three independent experiments. The values are means ± SD (n = 3). (For interpretation of color in Figs. 1–4 the reader is referred to the web version of this article.)

tagged pET modified vectors, including a tobacco etch virus (TEV) protease cleavage site. The internal loop residues from residue 134 to 149 were deleted in the CBSX1 Δloop mutant (Fig. 1B) and was designed based on the invisible density of the CBSX2 structure [23] in addition to analysis of the secondary structure prediction, disorder prediction, and the sequence alignment between CBSX1 and CBSX2. The Δloop mutant (insertion of a Gly residue between Ser134 and Asp150) was obtained by PCR using an enzyme-free cloning method [26]. GST-tagged CBSX1 mutants (R107A, K199A, and R202A) were obtained by PCR using QuikChange mutagenesis (Stratagene).

2.2. Protein expression and purification

Escherichia coli BL21 (DE3) cells were used to express all the recombinant proteins. Cells were grown in LB medium with kanamycin (50 μg/ml) at 37 °C to an $OD_{600\,nm}$ of 0.7, induced by the addition of 0.5 mM IPTG, and maintained for 20 h at 18 °C. The cells were harvested by centrifugation for 20 min at 6000 rpm and re-suspended in phosphate buffered saline (PBS) containing 1 mM PMSF with one protease inhibitor cocktail tablet (Roche), and subsequently disrupted by ultrasonication. The lysates were collected by centrifugation for 1.5 h at 15,000 rpm. The GST-fused proteins (CBSX1, CBSX1 Δloop, and CBSX1 mutants) were incubated with GST Sepharose 4B resin (GE Healthcare) that had been pre-equilibrated with PBS. The resin was washed extensively with PBS and the protein was eluted from the resin with elution buffer (50 mM Tris–HCl pH 8.0, 20 mM NaCl, 1 mM DTT, and 10 mM reduced glutathione). CBSX proteins were released from the fusion protein by overnight digestion with a 1/50 (w/w) ratio of TEV protease at room temperature. Only one extra glycine residue was attached to the N-terminus of the CBSX proteins after TEV cleavage. Further purification was carried out by successive anion exchange (HiTrap Q Fast Flow, GE Healthcare) and size exclusion (Hiload 16/60 Superdex 75 pg, GE Healthcare) chromatography after being equilibrated with gel filtration buffer (20 mM HEPES pH 7.5, 100 mM NaCl and 1 mM EDTA). Free GST contaminants were removed by passing the digested sample over a GST-Sepharose column. The final proteins were concentrated to 10 mg/ml using a 10-kDa cut-off filter (Amicon Ultra). Trxs were purified in the same manner as that for the GST-fused CBSX proteins followed by size exclusion chromatography after being equilibrated with 20 mM Tris–HCl pH 7.7, 300 mM NaCl, and 1 mM EDTA.

2.3. Crystallization, data collection, and processing

Crystallization was performed using the hanging drop vapor diffusion method at 22 °C. The CBSX1 protein was crystallized and the data sets were collected using synchrotron radiation as previously described [25]. The initial crystallization condition for the CBSX1 Δloop was 0.1 M sodium acetate pH 4.6 and 2.0 M ammonium sulfate. The best crystals for the CBSX1 Δloop were obtained using 0.1 M sodium acetate pH 4.4 and 1.5 M ammonium sulfate. The CBSX1 crystals had a trigonal space group $P3_121$ with unit cell dimensions of $a = b = 56.36$ Å and $c = 82.60$ Å. Likewise, the CBSX1 Δloop crystals belonged to the same space group $P3_121$ with unit cell dimensions of $a = b = 55.82$ Å and $c = 83.00$ Å. The crystals were flash cooled in liquid nitrogen using a cryoprotectant solution containing reservoir buffer with 20% (w/v) glycerol. X-ray diffraction data of the CBSX1 and CBSX1 Δloops were collected on a beamline NW12A at Photon Factory, Tsukuba, Japan. All data sets were recorded using an ADSC Quantum 210r CCD detector and processed and integrated using DENZO, and scaled using SCALEPACK from the HKL-2000 program suite [27]. The crystal parameters and data collection statistics are summarized in Table 1.

Table 1
Data collection, phasing, and refinement statistics.

	CBSX1	Δloop mutant
Data collection		
X-ray source[a]	PF AR-NW12A	
Wavelength (Å)	0.97923	1.0000
Space group	$P3_121$	
Cell dimension		
a, *b*, *c* (Å)	56.36, 56.36, 82.60	55.82, 55.82, 83.00
α, β, γ (°)	90, 90, 120	90, 90, 120
Resolution (Å)[b]	2.40 (2.49–2.40)	2.20 (2.24–2.20)
Total reflections	63,521	118,758
Unique reflections	6,273	8,007
Completeness (%)[b]	99.4 (97.5)	99.9 (100.0)
Overall $(I/\sigma I)$[b]	60.8 (4.2)	64.8 (7.0)
R_{sym} (%)[b,c]	6.9 (41.2)	4.4 (47.3)
Refinement		
Resolution range (Å)	31.52–2.40	31.48–2.20
No. of reflections	6,329	7598
R_{work}/R_{free} (%)[d]	0.248/0.309	0.257/0.311
Number of atoms		
Proteins	946	1026
Water	34	30
Ions	0	0
RMS deviations		
Bond lengths (Å)	0.009	0.004
Bond angles (°)	1.190	0.728
Ramachandran outlier	0.0%	0.0%
PDB ID	4GQV	4GQW

[a] PF; Photon Factory, Japan.
[b] The values in parentheses are for reflections in the highest resolution bin.
[c] $R_{sym} = \Sigma_h\Sigma_i|I(h,i) - \langle I(h)\rangle|/\Sigma_h\Sigma_i\ I(h,i)$, where $I(h,i)$ is the intensity of the *i*th measurement of reflection *h* and $\langle I(h)\rangle$ is the corresponding average value for all *i* measurements.
[d] $R_{work} = \Sigma||F_o| - |F_c||/\Sigma|F_o|$, where R_{free} was calculated for the 10% test set of reflections.

2.4. Structure determination

All structures were solved by the molecular replacement (MR) method using the program PHASER [28] and refinement was carried out using PHENIX software [29]. Initial phases of the CBSX1 Δloop structure were calculated using a previously determined structure of CBSX2 from *A. thaliana* (PDB ID: 3SL7) as a search model [23]. The MR solution resulted in one monomer per asymmetric unit. The structure of CBSX1 Δloop was completed using successive cycles of manual rebuilding with COOT [30] followed by refinement using PHENIX [29]. The phases of the CBSX1 structure were then determined by MR using the refined CBSX1 Δloop structure as a search model. The model was further refined using PHENIX, and model rebuilding and solvent addition were performed with COOT [30]. The model geometry and the secondary structural elements were assessed using the PROCHECK program [31]. All figures were generated using PyMOL (http://www.pymol.org).

2.5. Enzymatic assay

Trx activity was measured as described [23,32] for 1 h at 24 °C and defined as the maximal rate of increase in turbidity at 650 nm due to insulin precipitation. CBSX proteins were used at a final concentration of 20 μM in 100 μl 0.1 M HEPES pH 7.0, 1 mM EDTA, 10 μM Trx, 2 mM DTT, and 160 μM bovine insulin (Sigma–Aldrich Inc.). Adenosine derivatives (1 mM) were used as a cofactor and the same buffer without CBSXs was used as a reference.

3. Results and discussion

3.1. Structure determination

CBSX1 crystals were previously obtained and had a $P3_121$ space group or its enantiomorphic pair $P3_221$ [25]. Several data sets were collected for MAD and MIR phasing. However, the phase problem was not successfully overcome due to the failure to locate anomalous scatters or heavy atoms. After we determined the structure of CBSX2 using MAD phasing [23], structure determination of CBSX1 was attempted using the MR method with the refined CBSX2 structure as a search model. Although the CBSX1 structure was expected to be very similar to that of CBSX2 based on high sequence conservation (Fig. 1A), the initial attempt to solve the CBSX1 structure by MR was not straightforward due to structural differences in the overall shape (see below for details). The CBSX2 structure is similar to the known CBS domain structure [33]. However, it contains a characteristic additional α-helix (α5) followed by an invisible region and a C-terminal helix α8 that does not exist in other CBS domain structures [23,33]. We found that the invisible region from CBSX2 is not necessary for core folding of CBSXs, and therefore we designed a Δloop mutant CBSX1 for improved crystals (Fig. 1B). This deletion mutant was cloned, over-expressed, purified, and crystallized. The purified Δloop mutant showed the same effect on Trx activation as wild-type CBSX1, which suggested that the deleted loop is not involved in the interaction with Trx (Fig. 1C). Interestingly, the Δloop mutant belongs to the same crystal system with better resolution (Table 1) and the structure of the CBSX1 Δloop mutant was determined by the MR method using the refined CBSX2 structure. Finally, the crystal structure of CBSX1 was determined by MR using the CBSX1 Δloop structure as a search model and refined to a resolution of 2.4 Å. The final R_{free} values for the refined structures were relatively high. This is most probably due to the absence of a significant portion of the polypeptide chain, which cannot be built into the invisible electron density map. However, the two structures CBSX1 and CBSX1 Δloop were well refined with good stereochemistry and Ramachandran results (Table 1).

3.2. Overall structures of CBSX1

The crystal structure of CBSX1 is similar to that of CBSX2 (Fig. 2). There is one molecule in the asymmetric unit and it forms a homodimer (Fig. 2A) with a symmetry-operated molecule. CBSX1 consists of two conserved CBS domains, and it contains two central β-strands (β1-β2 and β3-β4) and it is flanked by six α-helices (Fig. 2B). The first CBS domain (CBS1) contains a characteristic α-helix (α5) in the CBSX2 structure. This additional helix is followed by an invisible loop region in CBSX2 (Fig. 2C) and the CBSX1 Δloop (Fig. 2D). The electron density map around the α5 helix region is invisible in CBSX1, which is suggestive of its flexible nature. CBSX1 possesses a shorter C-terminal helix α8 than CBSX2 and the CBSX1 Δloop, and this last helix plays an important role in the dimerization of both CBSX1 and CBSX2 (Fig. 2A) [23]. The key structural features of CBSX1 are an anti-parallel dimeric assembly (CBS1 interacts with CBS2′ and CBS2 interacts with CBS1′) and a unique bend along the side of the molecule (Fig. 3A). Similar features were previously identified in CBSX2 [23]. The bending angle of CBSX1 is approximately 155° (Fig. 2C), which is wider than that of CBSX2, which is approximately 125° (Fig. 3B). The bending angle for the CBSX1 Δloop is also similar to that of CBSX1, which suggests that this bending is not due to the unique insertion region. This feature contrasts with all other parallel and anti-parallel CBS domain proteins, which are characterized by a 180° flat structure along the side [15,21,23].

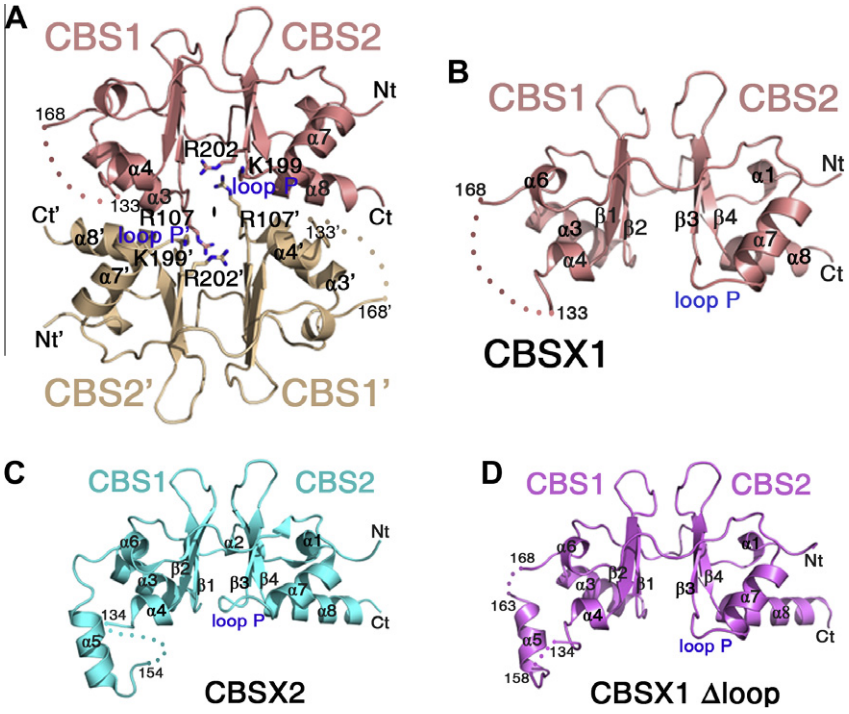

Fig. 2. (A) The overall structure of dimeric CBSX1 viewed along the twofold molecular symmetry axis. Subunits for the A and B chains are colored salmon and wheat, respectively. For clarity, prime (′) has been added to all of the labels for chain B. (B–D) Ribbon diagram showing the monomeric subunit of CBSX1 (B), CBSX2 (C), and the CBSX1 Δloop (D) colored salmon, cyan, and magenta, respectively. The secondary structural elements are sequentially labeled, and invisible residues (from 134 to 167 for CBSX1, from 135 to 153 for CBSX2, and from 135 to 157 and from 164 to 167 for the CBSX1 Δloop) are indicated as dots. The loop toward the pocket is labeled 'loop P'. The N- and C-termini of CBSX proteins, the first CBS domain, and the second CBS domain are labeled Nt, Ct, CBS1, and CBS2, respectively. (For interpretation of the references to colour in this figure legend, the reader is referred to the web version of this article.)

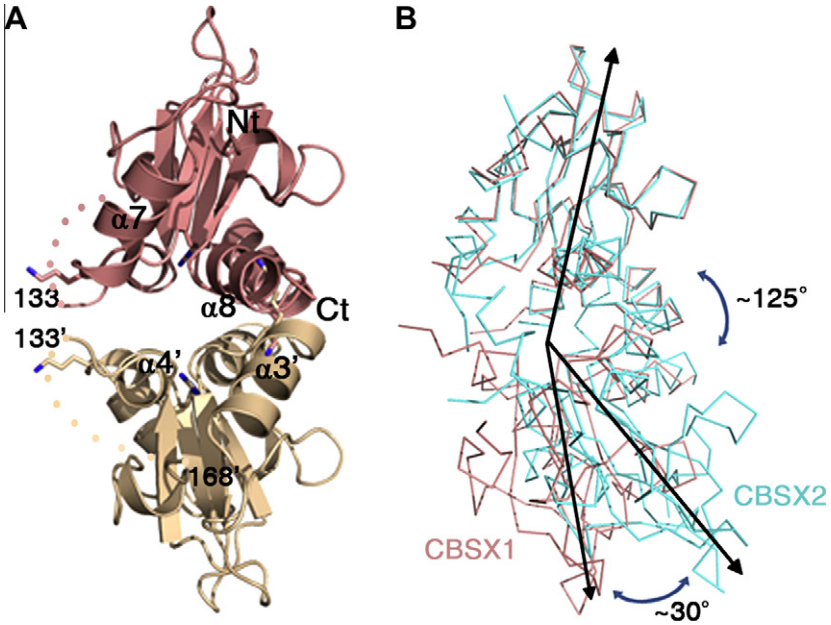

Fig. 3. (A) A 90° rotation along the vertical axis of the view of Fig. 2A showing the side of the CBSX1 structure. Subunits for the A and B chains are colored salmon and wheat, respectively. For clarity, prime (′) has been added to all of the labels for chain B. (B) Superposition of the Cα structures of CBSX1 and CBSX2 viewed along the side of the molecule. CBSX1 and CBSX2 are colored salmon and cyan, respectively. The angles between CBSX2 and CBSX1 are indicated in degrees. (For interpretation of the references to colour in this figure legend, the reader is referred to the web version of this article.)

3.3. Putative AMP recognition region

The recognition motif (the conserved CBS-motif Ghx(S/T)x(S/T)D, where x is any amino acid and h is hydrophobic) for the ribose-phosphate moiety of the molecule such as AMP or ATP was identified based on sequence analyses of CBSX1 and CBSX2 [18]. The recognition motif of the CBS1 domains in CBSX1 and CBSX2 consist of residues $_{122}$GLVSDYD$_{128}$ and $_{124}$GVVSDYD$_{130}$ on

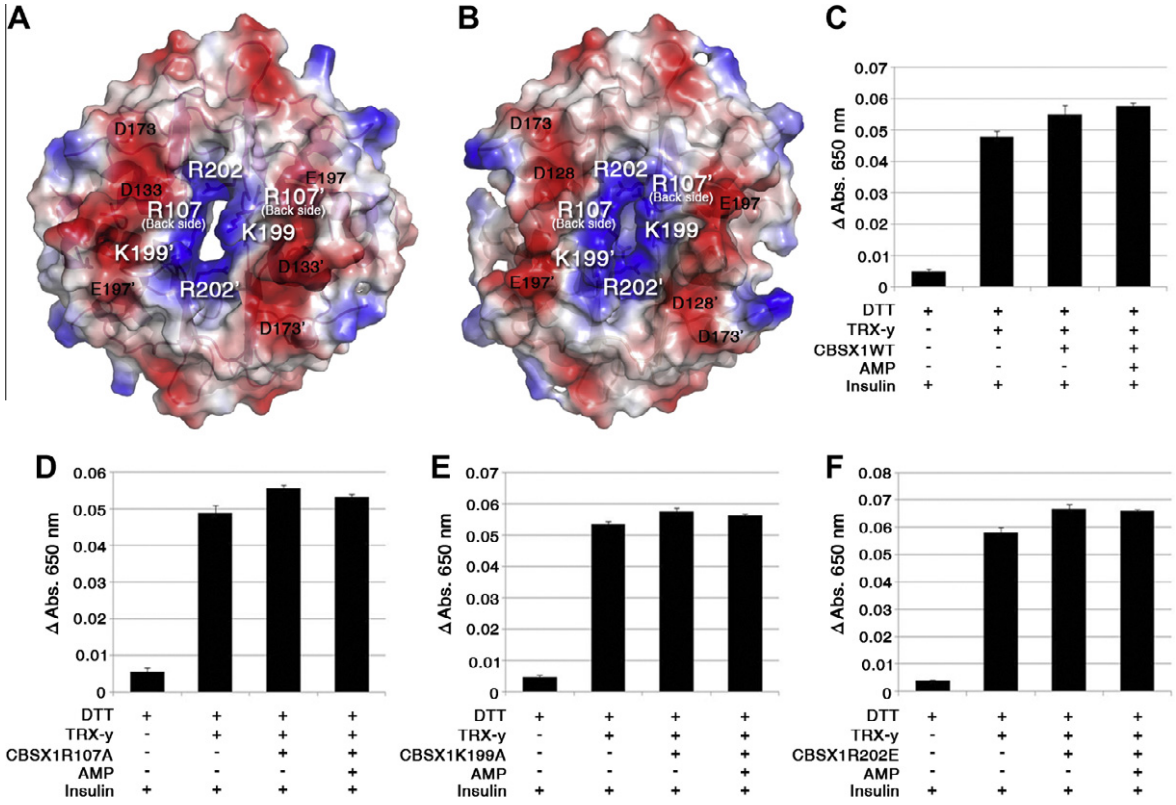

Fig. 4. (A, B) Transparent potential surface of dimeric CBSX1 (A) and the CBSX1 Δloop (B). Positive and negative electrostatic potentials are shown in blue and red, respectively. Selected residues are labeled. (C–F) Assay using insulin for the reducing activity of Trx-y in the presence of CBSX1 wild-type (WT) and mutant proteins (R107A, K199A, and R202E) as measured by the difference in absorbance at 650 nm. The error bars were calculated based on three independent experiments. The values are means ± SD (n = 3). (For interpretation of the references to colour in this figure legend, the reader is referred to the web version of this article.)

strand β2 and helix α4, respectively (Fig. 1A). We previously assayed the enzymatic activity of Trx, which is a downstream effector molecule of CBSXs, in the presence of three different nucleotides and found that only AMP enhanced Trx activity [23]. The negatively charged phosphate moiety of AMP is recognized by highly positively charged residues. Such a surface property has been found in other CDCPs from mammals and microbes as well as another family of ATP or AMP binding enzymes [11,15,17,18,33–37]. The dimeric CBSXs exhibit a disk-like structure with a central hole or large pocket that is formed by the two monomers (Fig. 2A). There is a loop ('loop P') on each CBSX monomer that closes the central hole in the center of the dimer (Fig. 2A). Near the central hole, a positively charged pocket that is formed along the twofold molecular axis was identified in CBSX1 (Fig. 4A). The electrostatic potential surface of the CBSX1 Δloop is very similar to that of full-length CBSX1. The central hole is not clearly formed because the conformations of loop P are slightly different (Fig. 2B and D) and the extended side chains near the twofold molecular center show different orientations (Fig. 4B). In particular, the conformation of loop P in CBSX2 is markedly different from that in CBSX1 (Fig. 2C) and the length of the loop is also different (Fig. 1A), suggesting the flexible nature of this region for accommodating incoming AMP ligands.

3.4. Biochemical data confirming the AMP binding site

To dissect the CBSX-AMP binding further, we mutated positively the residues, R107A, K199A, and R202E at the characteristic putative AMP binding site (Fig. 4A). All of these CBSX1 mutants enhanced the Trx activity similar to the wild-type protein (Fig. 4C–F), ruling out the interaction between this region of CBSX and Trx. Nevertheless, these mutants showed no AMP effect, which suggests that the AMP binding affinity may have deteriorated. The important question is how ligands such as adenine nucleotides regulate the function of the CBS domain. To understand this molecular mechanism, we need structures of the CBS domain in an apo form as well as in complexes with ligands. Another key question is the mode of interaction between CBSX and Trx. A unique insertion region in CBSX1, which is invisible in the electron density map due to its flexible nature, does not play a critical role in the Trx interaction since the Δloop mutant showed full activity relative to the wild-type (Fig. 1C). Thus far, all of the aforementioned three CBSX1 mutants had no effect on Trx activity. Therefore, for a complete understanding of the regulation of the Trx system by CBSXs, extensive biochemical and structural studies on the binary CBSX-Trx as well as the ternary CBSX-AMP-Trx complex are required.

Acknowledgments

We thank the staff at AR-NW12A beamline, Photon Factory, Japan for helping us with the data collection. This work was supported by a National Research Foundation of Korea (NRF) grant that was funded by the Korean Government (MEST; 2011-0028168) and the Korea Healthcare Technology R&D Project, Ministry for Health, Welfare & Family Affairs, Republic of Korea (A092006).

References

[1] S. Ignoul, J. Eggermont, CBS domains: structure, function, and pathology in human proteins, Am. J. Physiol. Cell Physiol. 289 (2005) C1369–1378.

[2] A. Bateman, The structure of a domain common to archaebacteria and the homocystinuria disease protein, Trends Biochem. Sci. 22 (1997) 12–13.

[3] X. Shan, R.L. Dunbrack Jr., S.A. Christopher, W.D. Kruger, Mutations in the regulatory domain of cystathionine beta synthase can functionally suppress patient-derived mutations in cis, Hum. Mol. Genet. 10 (2001) 635–643.

[4] M.H. Gollob, M.S. Green, A.S. Tang, et al., Identification of a gene responsible for familial Wolff–Parkinson–White syndrome, N Engl. J. Med. 344 (2001) 1823–1831.

[5] A. Kennan, A. Aherne, A. Palfi, et al., Identification of an IMPDH1 mutation in autosomal dominant retinitis pigmentosa (RP10) revealed following comparative microarray analysis of transcripts derived from retinas of wild-type and Rho(−/−) mice, Hum. Mol. Genet. 11 (2002) 547–557.

[6] B.E. Kemp, Bateman domains and adenosine derivatives form a binding contract, J. Clin. Invest. 113 (2004) 182–184.

[7] M. Pusch, Myotonia caused by mutations in the muscle chloride channel gene CLCN1, Hum. Mutat. 19 (2002) 423–434.

[8] R. Zhang, G. Evans, F.J. Rotella, E.M. Westbrook, D. Beno, E. Huberman, A. Joachimiak, F.R. Collart, Characteristics and crystal structure of bacterial inosine-5′-monophosphate dehydrogenase, Biochemistry 38 (1999) 4691–4700.

[9] R. Townley, L. Shapiro, Crystal structures of the adenylate sensor from fission yeast AMP-activated protein kinase, Science 315 (2007) 1726–1729.

[10] G.A. Amodeo, M.J. Rudolph, L. Tong, Crystal structure of the heterotrimer core of Saccharomyces cerevisiae AMPK homologue SNF1, Nature 449 (2007) 492–495.

[11] B. Xiao, M.J. Sanders, E. Underwood, et al., Structure of mammalian AMPK and its regulation by ADP, Nature 472 (2011) 230–233.

[12] M. Koutmos, O. Kabil, J.L. Smith, R. Banerjee, Structural basis for substrate activation and regulation by cystathionine beta-synthase (CBS) domains in cystathionine {beta}-synthase, Proc. Natl. Acad. Sci. USA 107 (2010) 20958–20963.

[13] M. Hattori, Y. Tanaka, S. Fukai, R. Ishitani, O. Nureki, Crystal structure of the MgtE Mg2+ transporter, Nature 448 (2007) 1072–1075.

[14] L. Feng, E.B. Campbell, Y. Hsiung, R. MacKinnon, Structure of a eukaryotic CLC transporter defines an intermediate state in the transport cycle, Science 330 (2010) 635–641.

[15] H. Tuominen, A. Salminen, E. Oksanen, et al., Crystal structures of the CBS and DRTGG domains of the regulatory region of Clostridiumperfringens pyrophosphatase complexed with the inhibitor AMP, and activator, diadenosine tetraphosphate, J. Mol. Biol. 398 (2010) 400–413.

[16] M. Proudfoot, S.A. Sanders, A. Singer, et al., Biochemical and structural characterization of a novel family of cystathionine beta-synthase domain proteins fused to a Zn ribbon-like domain, J. Mol. Biol. 375 (2008) 301–315.

[17] I. Gomez-Garcia, I. Oyenarte, L.A. Martinez-Cruz, The crystal structure of protein MJ1225 from Methanocaldococcus jannaschii shows strong conservation of key structural features seen in the eukaryal gamma-AMPK, J. Mol. Biol. 399 (2010) 53–70.

[18] M. Lucas, J.A. Encinar, E.A. Arribas, et al., Binding of S-methyl-5′-thioadenosine and S-adenosyl-L-methionine to protein MJ0100 triggers an open-to-closed conformational change in its CBS motif pair, J. Mol. Biol. 396 (2010) 800–820.

[19] M.D. Miller, R. Schwarzenbacher, F. von Delft, et al., Crystal structure of a tandem cystathionine-beta-synthase (CBS) domain protein (TM0935) from Thermotoga maritima at 1.87 A resolution, Proteins 57 (2004) 213–217.

[20] N.P. King, T.M. Lee, M.R. Sawaya, D. Cascio, T.O. Yeates, Structures and functional implications of an AMP-binding cystathionine beta-synthase domain protein from a hyperthermophilic archaeon, J. Mol. Biol. 380 (2008) 181–192.

[21] P. Ragunathan, T. Kumarevel, Y. Agari, A. Shinkai, S. Kuramitsu, S. Yokoyama, K. Ponnuraj, Crystal structure of ST2348, a CBS domain protein, from hyperthermophilic archaeon Sulfolobus tokodaii, Biochem. Biophys. Res. Commun. 375 (2008) 124–128.

[22] M.L. Sharpe, C. Gao, S.L. Kendall, E.N. Baker, J.S. Lott, The structure and unusual protein chemistry of hypoxic response protein 1, a latency antigen and highly expressed member of the DosR regulon in Mycobacterium tuberculosis, J. Mol. Biol. 383 (2008) 822–836.

[23] K.S. Yoo, S.H. Ok, B.C. Jeong, K.W. Jung, M.H. Cui, S. Hyoung, M.R. Lee, H.K. Song, J.S. Shin, Single cystathionine beta-synthase domain-containing proteins modulate development by regulating the thioredoxin system in arabidopsis, Plant Cell 23 (2011) 3577–3594.

[24] H.R. Kushwaha, A.K. Singh, S.K. Sopory, S.L. Singla-Pareek, A. Pareek, Genome wide expression analysis of CBS domain containing proteins in *Arabidopsis thaliana* (L.) Heynh and *Oryza sativa* L. reveals their developmental and stress regulation, BMC Genom. 10 (2009) 200.

[25] B.C. Jeong, K.S. Yoo, K.W. Jung, J.S. Shin, H.K. Song, Purification, crystallization and preliminary X-ray diffraction analysis of a cystathionine beta-synthase domain-containing protein, CDCP2, from Arabidopsis thaliana, Acta. Crystallogr. Sect. F. Struct. Biol. Cryst. Commun. 64 (2008) 825–827.

[26] D. Tillett, B.A. Neilan, Enzyme-free cloning: a rapid method to clone PCR products independent of vector restriction enzyme sites, Nucl. Acids Res. 27 (1999) e26.

[27] Z. Otwinowski, W. Minor, Processing of X-ray diffraction data collected in oscillation mode, Methods Enzymol. 276 (1997) 301–326.

[28] A.J. McCoy, R.W. Grosse-Kunstleve, P.D. Adams, M.D. Winn, L.C. Storoni, R.J. Read, Phaser crystallographic software, J. Appl. Crystallogr. 40 (2007) 658–674.

[29] P.D. Adams, P.V. Afonine, G. Bunkoczi, et al., PHENIX: a comprehensive Python-based system for macromolecular structure solution, Acta. Crystallogr. D. Biol. Crystallogr. 66 (2010) 213–221.

[30] P. Emsley, B. Lohkamp, W.G. Scott, K. Cowtan, Features and development of Coot, Acta. Crystallogr. D. Biol. Crystallogr. 66 (2010) 486–501.

[31] R.A. Laskowski, M.W. MacArthur, D.S. Moss, J.M. Thornton, PROCHECK: a program to check the stereochemical quality of protein structures, J. Appl. Crystallogr. 26 (1993) 283.
[32] C. Laloi, N. Rayapuram, Y. Chartier, J.M. Grienenberger, G. Bonnard, Y. Meyer, Identification and characterization of a mitochondrial thioredoxin system in plants, Proc. Natl. Acad. Sci. USA 98 (2001) 14144–14149.
[33] A.A. Baykov, H.K. Tuominen, R. Lahti, The CBS domain: a protein module with an emerging prominent role in regulation, ACS Chem. Biol. 6 (2011) 1156–1163.
[34] H.K. Song, C. Hartmann, R. Ramachandran, M. Bochtler, R. Behrendt, L. Moroder, R. Huber, Mutational studies on HslU and its docking mode with HslV, Proc. Natl. Acad. Sci. USA 97 (2000) 14103–14108.
[35] E.Y. Park, S.I. Oh, M.J. Nam, J.S. Shin, K.N. Kim, H.K. Song, Crystal structure of 5′-methylthioadenosine nucleosidase from *Arabidopsis thaliana* at 1.5-A resolution, Proteins 65 (2006) 519–523.
[36] S.B. Hong, B.W. Kim, K.E. Lee, S.W. Kim, H. Jeon, J. Kim, H.K. Song, Insights into noncanonical E1 enzyme activation from the structure of autophagic E1 Atg7 with Atg8, Nat. Struct. Mol. Biol. 18 (2011) 1323–1330.
[37] M. Bochtler, C. Hartmann, H.K. Song, G.P. Bourenkov, H.D. Bartunik, R. Huber, The structures of HslU and the ATP-dependent protease HslU-HslV, Nature 403 (2000) 800–805.